catalysts

MDPI

Article

Hydrothermal Synthesis of CuO/RuO_2/MWCNT Nanocomposites with Morphological Variants for High Efficient Supercapacitors

Yi-Chen Chung [1,†], Ade Julistian [1,†], Lakshmanan Saravanan [1,2,*], Peng-Ren Chen [1], Bai-Cheng Xu [1], Pei-Jie Xie [1] and An-Ya Lo [1,*]

[1] Department of Chemical and Materials Engineering, National Chin-Yi University of Technology, Taichung 411030, Taiwan; zxczxazxsbnm@gmail.com (Y.-C.C.); ade.julistian@gmail.com (A.J.); b224466885@gmail.com (P.-R.C.); ples510777@gmail.com (B.-C.X.); eugene1779@gmail.com (P.-J.X.)

[2] Department of Micro and Nanoelectronics, Saveetha School of Engineering, Saveetha Institute of Medical and Technical Sciences (SIMATS), Thandalam 602105, India

* Correspondence: ljsaravanan08@gmail.com (L.S.); aylo@ncut.edu.tw (A.-Y.L.)

† These authors contributed equally to this work.

Abstract: In this study, we develop the optimum composition of copper oxide/ruthenium oxide and multi-walled carbon nanotubes (CuO/RuO_2/MWCNTs) ternary nanocomposite via a hydrothermal method as an efficient electrode material for supercapacitor applications. The ratio between CuO and RuO_2 varied to improve the electrochemical performance of the electrode. The synthesized nanocomposites are analyzed by high-resolution scanning electron microscopy (HR-SEM), thermo gravimetric analyzer (TGA) and electrochemical impedance spectroscopy (EIS). Furthermore, the elemental composition is analyzed by energy dispersive X-ray (EDX) spectroscopy and the specific capacitance was analyzed by cyclic voltammetry (CV) and galvanostatic charge–discharge (GCD) methods. The electrochemical investigations is conducted in a three-electrode system and the sample is attached on a stainless steel plate as the working electrode; platinum wire works as the counter electrode and Ag/AgCl electrode as the reference electrode, adopting 3 M $(NH_4)_2SO_4$ as the electrolyte. The resultant of CuO/RuO_2/MWCNT nanocomposite with 7 wt% Cu and 20 wt% Ru was found to perform the highest specific capacitance of 461.59 F/g in a current density of 1 A/g.

Keywords: nanocomposite; metal oxides; MWCNTs; scanning electron microscopy; supercapacitor

Citation: Chung, Y.-C.; Julistian, A.; Saravanan, L.; Chen, P.-R.; Xu, B.-C.; Xie, P.-J.; Lo, A.-Y. Hydrothermal Synthesis of CuO/RuO_2/MWCNT Nanocomposites with Morphological Variants for High Efficient Supercapacitors. *Catalysts* **2022**, *12*, 23. https://doi.org/10.3390/catal12010023

Academic Editor: Hamidreza Arandiyan

Received: 1 December 2021
Accepted: 23 December 2021
Published: 26 December 2021

1. Introduction

There is an increasing demand for environmentally friendly technologies that reduce CO_2 production in various manners, such as fuel cells, solar cells, CO_2 reduction and supercapacitors [1–3]. Among all those technologies, the supercapacitor is an inimitable energy storage device with a high performance and rechargeable energy storage/conversion devices that is in imperative need in the current industry [3,4]. Therefore, supercapacitors have been recognized as a potential storage device for the next generation owing to their greater power density, high-power density and great cycle stability at a reduced cost [3,5–7]. The performance of supercapacitors depends on several factors, such as the electrochemical characteristics of the electrode materials, the electrolytes and voltage window [8,9]. There is an important category of supercapacitors called hybrid supercapacitors that combine electric double layer capacitances (EDLCs: carbon-based materials) and pseudo-capacitance (transition metal oxides) [10–12]. Both faradaic and non-faradaic pathways work during charge-discharge process. Therefore, hybrid supercapacitors are known to achieve both high energy and high-power densities.

Recently, transition metal oxides (TMOs) have received much attention, which is accounted for by their low cost and rich redox chemistry [4,13]. Specifically, the single and bimetallic TMOs exhibited high specific power and specific capacitance [14]. Among various TMOs, ruthenium oxide, with its two distinct adsorption sites on the surface, has been widely identified as a promising material for electrochemical storage devices,

owing to its high specific capacitance, chemical activity and having good reversibility and stability [15–17]. RuO_2 possess surprising feature for pseudo-capacitance, such as rapid proton transfer, exceptional reversible redox transitions, and excellent specific capacitance (900–1400 F/g) [18]. Ye et al. prepared a RuO_2/MWCNT nanocomposite using magnetic sputter deposition using an expensive Ru target [19]. However, high priced ruthenium precursors, toxicity, and limited abundance restrict its commercial usage. It was also reported that the hydrothermal method of synthesizing nanocomposites will significantly enhance the electric capacitive performance and RuO_2 utilization in the supercapacitor [20]. The major disadvantage of ruthenium oxide materials is their easy agglomeration, which severely affect the electrochemical performance. The strategy to exert nanoparticles (NPs) is appreciated due to their large specific surface area and the reduction of bulk atoms involved in the faradaic reactions. However, the NPs have a strong trend to agglomerate, thus usually leading to the loss of the accessible surface for the electrolyte. Hybridization with carbon-based materials is considered the most potential strategy to improve the dispersion of ruthenium oxides [17,21]. Among the conducting materials with a higher specific surface area, both carbon nanotubes (CNTs) and mesoporous carbon materials are good candidates of EDLC owing to their unique properties, such as good electrical conductivity and high specific surface area. The CNTs possesses higher electronic conductivity than mesoporous carbon materials.

Copper oxide (CuO) is a *p*-type semiconductor with a direct band gap of 1.2 eV (bulk) with its nanostructures having large surface area [22]. In spite of the good theoretical capacitance, CuO suffers low poor kinetics and cyclic performance because of low conductivity and pulverization due to volume expansion during cycling, resulting in unsatisfactory performances and limiting its applications [23]. Moreover, incorporating pseudocapacitive materials into copper oxides can enhance the low specific capacitance value to advance the process of charging transfer [24]. Recently, Wang et al. have prepared copper oxide/cuprous oxide/carbon (CuO_x@C) nanocomposites using a hydrothermal method to provide precise diffusion pathways for fast reaction kinetics [25].

The pseudocapacitive performance of the electrode materials is mostly dependent on the synthesizing methods and its morphology. It has been reviewed that the electrical performance of the electrode increases with the addition of optimum metal oxides contents, and also identified that the subsequent oxide loading will destroy the high surface area structure [26]. Earlier, Cui and his co-workers reported the preparation of a mesostructured CuO/RuO_2 bimetal oxide nanocomposite to achieve a high catalytic activity toward ammonia oxidation [27]. The current investigation mainly focuses on utilizing the pseudocapacitive metal oxides, such as ruthenium oxide and copper oxide (RuO_2 and CuO) NPs, in a hybrid nanocomposite and upholding the synergistic effect from these binary metal oxides with the highly conductive carbon support (MWCNTs), to obtain better electrochemical signatures. In this paper, the influence of blending ruthenium oxide and copper oxide with MWCNTs to prepare a ternary nanocomposite, by varying the metal ratio of ruthenium (Ru) and copper (Cu), on capacitive behavior is discussed in detail.

2. Experimental

2.1. Materials

MWCNTs were purchased from Hodogaya chemicals. Similarly, the cupric acetate monohydrate ($Cu(CH_3COO)_2 \cdot H_2O$, 98.0%) and ruthenium (III) chloride hydrate ($RuCl_3 \cdot xH_2O$, 42.00%) were ordered from BAKER ANALYZED®. The electrolyte ammonium sulfate ($(NH_4)_2SO_4$, 99.5%) was purchased from ACROS Organics™; the solvents sodium hydroxide (NaOH) and ethanol (C_2H_6O, 99.5%) purchased from ACROS Organics™ and ECHO Chemical, respectively; and N-methylpyrrolidone (C_5H_9NO, 99.5%) was obtained from M-Tedia®. All the solvents were AR grade and could be used without further purification.

2.2. Functionalization of MWCNTs

To remove the hydrophobicity of MWCNTs, an acid treatment is necessary to obtain a hydrophilic group (oxygen-containing groups) on the surface of MWCNTs. This method allows the MWCNTs to disperse homogenously in the solution and remove the impurities. It helps to increase the surface activity of MWCNTs and the ability to absorb ions. A total of 2 g of MWCNTs was added into 500 mL strong acid solution of a mixture, containing H_2SO_4 and HNO_3 (3:1). The mixture of MWCNTs with the acid was stirred for 24 h at 80 °C. Then, the solution was filtered and washed with DI water until the pH value was 7. It dried in the oven at 70 °C for 48 h for further processing to synthesize the CuO/RuO_2/MWCNT nanocomposites. The oxygenated functional groups on the MWCNTs improve the hydrophilicity of carbon surface [28].

2.3. Preparation of CuO/RuO_2/MWCNT Nanocomposites

First of all, a copper oxide, ruthenium oxide and MWCNTs (CuO/RuO_2/MWCNT) nanocomposite was synthesized by the hydrothermal method. In a typical experiment, 30 mg of functionalized MWCNTs was dispersed in 40 mL of DI water in ultrasonic bath for 1 h to obtain a better homogenous solution.

In line with the preparation of the MWCNT solution, to prepare the metallic solution, the optimum mole concentration of cupric acetate monohydrate and ruthenium chloride hydrate was mixed in N-methylpyrrolidone (NMP; 1 g) in 20 mL of DI water solution. An equal volume concentration was used for metal and MWCNTs. The NMP in metallic solution served as a surfactant to facilitate the dissolution of metals by stirring it for 30 min. In the next step, the 2 solutions were mixed by stirring for 10 min. To obtain a better dispersion, the mixed solution was treated in an ultrasonic bath for 1 h. Then, the aqueous 1 M NaOH solution was added drop wise until the pH value reached above 9 and the solution was stirred for 10 min to maintain it in an alkaline condition. Additionally, NaOH also plays a role in the intermediate reaction in the formation of metal oxide NPs. The solution was then loaded into a Teflon-lined autoclave and placed in a furnace at 180 °C for 12 h, and the autoclave was cooled down to room temperature to produce the metal oxide NPs/MWCNT nanocomposite. The washing process was performed by centrifuging at 6000 rpm, using DI water and ethanol for three times to remove the impurities. Then, the final product of CuO/RuO_2/MWCNT nanocomposite was collected after being dried in a 70 °C oven for 1 day.

2.4. Material Characterization Techniques

The morphologies and elemental composition of each nanocomposite sample was examined by scanning electron microscope (FESEM; JSM-5410). TGA measurements were performed to examine the thermal stability of all the nanocomposite samples and the total amount of CuO and RuO_2 by using thermal gravimetric analysis (TA-Q500). The measurements were performed with a heating rate of 15 °C/min from RT and 800 °C under air.

Cyclic voltammetry (CV, potential range 0–1.0 V, sweep rate 5–200 $mV{\cdot}s^{-1}$), electrochemical impedance spectroscopy (EIS, 10 mHz to 100 kHz, 5 mV amplitude) and galvanostatic charge/discharge (GCD) measurements were conducted using an electrochemical workstation (CHI 611E), in a three-electrode cell.

The gravimetric capacitances examined by CV and GCD measurements were calculated according to Equations (1) and (2), respectively. Similarly, the energy density (D_e) and (D_p) were calculated by Equations (3) and (4), respectively:

$$C_m = \frac{1}{2m(V_h - V_l)} \int I(V)dV \quad (1)$$

$$C_s = \frac{I \times \Delta t}{m \times \Delta V} \quad (2)$$

$$D_e = \frac{1}{2} C_s \left(\Delta V^2\right) \quad (3)$$

$$D_p = \frac{D_e}{\Delta t} \quad (4)$$

where I, Δt, m and ΔV represent the charge–discharge current, time differential, mass of the active electrode material and the voltage range of scanning segments, respectively.

For electrochemical studies, we used the half cell with three electrode configurations to test the electrode materials. The three electrode components were used as follows: the synthesized active (electrode) material was deposited on the stainless steel plate as the working electrode; the platinum wire was used as the counter electrode; and the Ag/AgCl electrode was used as the reference electrode. All the electrochemical examinations were carried out with 3 M ($(NH_4)_2SO_4$) as electrolyte. The active electrode material contained 10 wt% of polyvinylidene fluoride (PVDF) dissolved in N-methylpyrrolidone (NMP) as a conductive binder. The mass of active material used is 0.1 mg. Before the characterization, the deposited wet electrode needed to be dried in the oven to increase the contact between the active materials and the working electrode.

3. Results and Discussion

3.1. SEM Analysis

The SEM images of CuO/RuO_2/MWCNT (denoted as C_xR_yM hereafter, where the subscript x and y represent wt% of Cu and Ru rounded to one digit, respectively) nanocomposites revealed that CuO/RuO_2 NPs were well dispersed on the surface of the MWCNTs with uniform size and random directions. While more than 20 wt% Ru and 9 wt% Cu were added, Figures 1a–e and 2a–e, respectively, indicate that there are a lot of metal oxide NPs that started to stack together and began to cover the surface of the MWCNTs and form agglomerated structures.

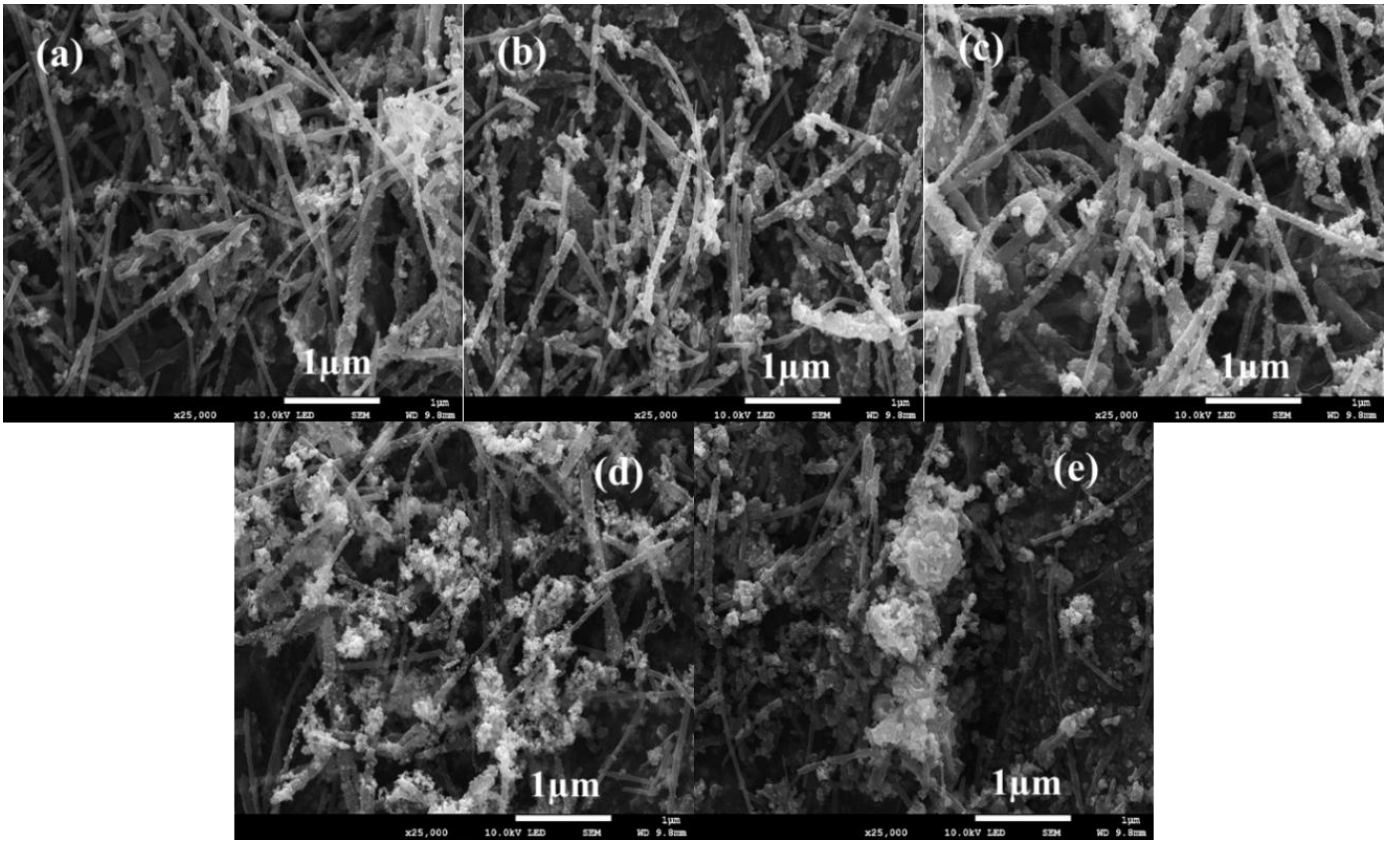

Figure 1. SEM images of C_{35}/R_yM electrodes with (**a**) 11, (**b**) 16, (**c**) 17, (**d**) 20 and (**e**) 23 wt% of Ru.

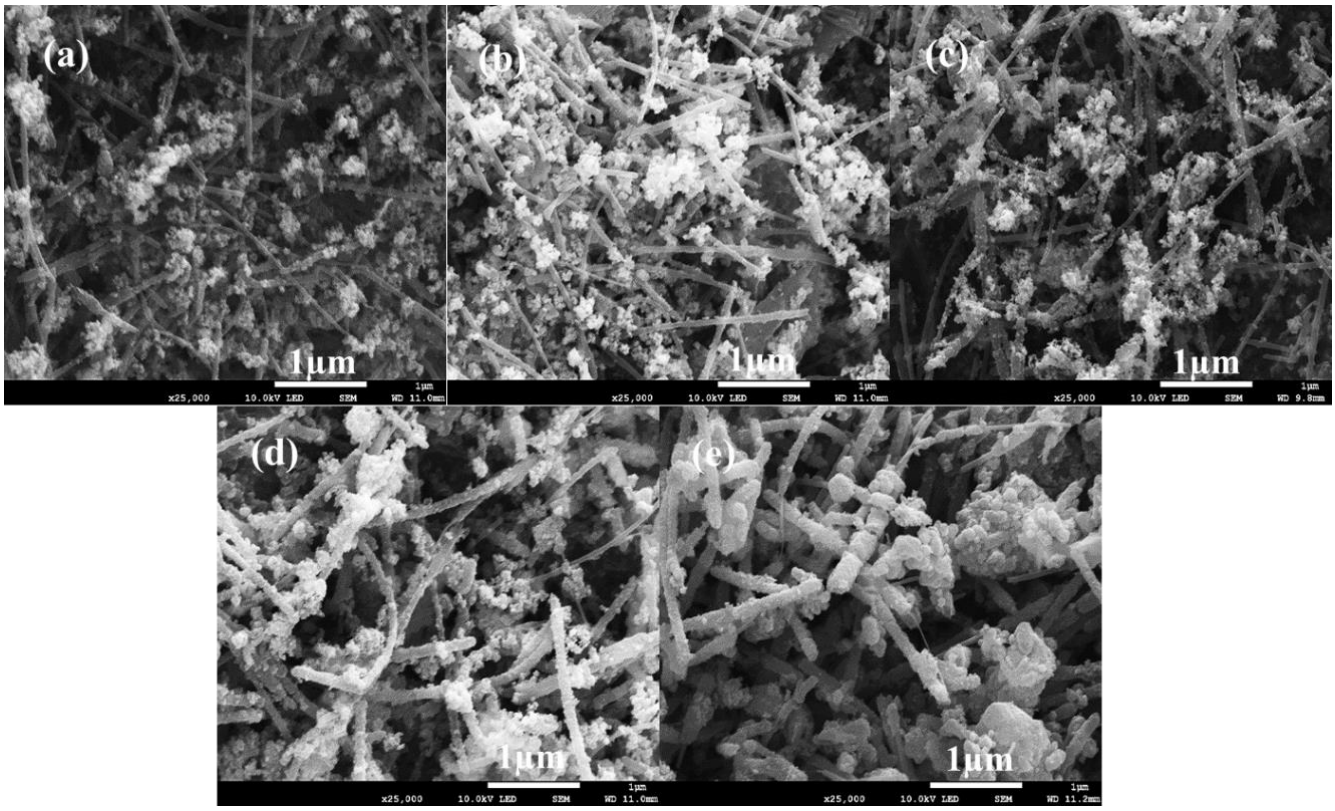

Figure 2. SEM images of $C_xR_{20}M$ electrodes with (**a**) 7, (**b**) 8, (**c**) 9, (**d**) 10 and (**e**) 11 wt% of Cu.

As we can see from the SEM images in Figures 1a–e and 2a–e, the growth pattern of RuO_2/CuO NPs on the surface of the MWCNTs appears to have a dissimilar morphology. That is, for higher concentrations, the oxide NPs in $C_{35}R_yM$ has shown a more agglomerate structure than their counterparts in $C_xR_{20}M$, which can be attributed to the extensive amount of Cu content. It is also evident that the surfaces of the MWCNTs became much rougher, indicating the high growth rate of RuO_2/CuO NPs on the MWCNT surfaces. The images clearly show that the nanotubes are coated with the NPs, and these particles are very small and highly dispersed on the whole surfaces of the MWCNTs, which has adverse effects on lowering its surface area. The resulting nanocomposites were further characterized using EDX to examine their chemical composition. EDX spectra validate the existence of Ru and Cu with different wt%. Figures S1 and S2 show the EDX-mapping of $C_{35}R_yM$ and $C_xR_{20}M$ composites, respectively. Additionally, they also display that CuO and RuO_2 were well distributed on the MWCNTs.

3.2. Thermo Gravimetric Analysis

Figure S5a,b displays the TGA curves of $C_{35}R_yM$ and $C_xR_{20}M$ nanocomposites with various content of Ru and Cu, respectively. The samples were heated in an air atmosphere with a heating rate of 15 °C/min from 25 °C to 800 °C. Various stages of degradation were observed in all the nanocomposite samples. In Figure S3a, the weight loss initiates at the temperature of around 50 °C. The first stage of weight loss emerges in the temperature range of 50–150 °C and is attributed to the removal of surface adsorbed water and is continuous in the second stage of degradation range up to 270 °C, with the significant weight loss in the samples. The third stage between 180 °C and 300 °C could be ascribed to the decomposition of all the hydrophilic functional groups still attached to the MWCNT surface after the functionalization process and the loss of water contained in RuO_2/CuO particles. While the additional weight loss curve detected between 600 °C and 800 °C relates to the complete oxidation of the nanotubes, it reveals that the higher content of oxide NPs plays a significant catalytic role in the rapid oxidation of MWCNTs. This is due

to the heat localization of metal NPs, which accelerate the heat transfer and increase the oxidation rate [29]. The residual weight percentage and the thermal stability of $C_{35}R_yM$ and $C_xR_{20}M$ were tabulated in Table S1 and Table S2, respectively.

3.3. Electrochemical Studies

To investigate the impacts of varying the concentration of metal oxides on the electrochemical performance of C_xR_yM nanocomposites, cyclic voltammetry (CV), galvanostatic charge–discharge (GCD) and electrochemical impedance spectroscopy (EIS) tests were performed. The applied potential was between −0.5 V to 0.5 V at a fixed scan rate of 10 mV·s^{-1}, and the GCD analysis was conducted at a current density of 1 A·g^{-1} with a potential between −0.5 V and 0.5 V. A slow scan rate was used to accelerate the large number of protons that approach the electrode surface, which yields a high capacitance and, in the case of high scan rate, the possibility of protons to approach the electrode surface is less, resulting in low specific capacitance [30]. The charge/discharge current applied was 0.1 mA. EIS analysis was performed to observe the effect of the metal oxide on the electrical resistivity of the nanocomposite.

To approach optimized Cu and Ru contents, in this study, three sets of experiments were adopted. First of all, the Cu content was optimized without the existence of Ru. Figure S4a,b and Table S3 show the CV and GCD curves for the C_xR_0M nanocomposites. As the results, 35 wt% of Cu was found with the best specific capacitance of 104.7 F/g.

Secondly, the Ru content was then optimized with the presence of 35 wt% Cu on the MWCNTs. Figure 3a,b respectively shows the CV and GCD curves for the $C_{35}R_yM$ nanocomposites with the addition of a different Ru content. All the CV curves look different from ideal rectangular shape with clear redox peaks, which indicates that all the electrodes exhibit a pseudocapacitive nature. As shown in Figure 3a, the voltammetric current was significantly enhanced when the Ru content increased in $C_{35}R_yM$ electrodes. It also indicates that the charge storage characteristic of the pseudocapacitive process is from the reversible redox reactions of Cu (I) ↔ Cu(II) and Ru (VI) ↔ Ru (II). In the case of RuO_2, it can store charge through the reversible redox reactions in the acidic electrolyte, where the oxidation states of Ru alter from $Ru^{(IV)}$ to $Ru^{(II)}$. as shown below [31,32]:

$$RuO_2 + zH^+ + ze^- \leftrightarrow RuO_{2-z}(OH)_z;\ 0 \le z \le 2 \quad (5)$$

where z denotes the average electron transfer number involved in the reaction.

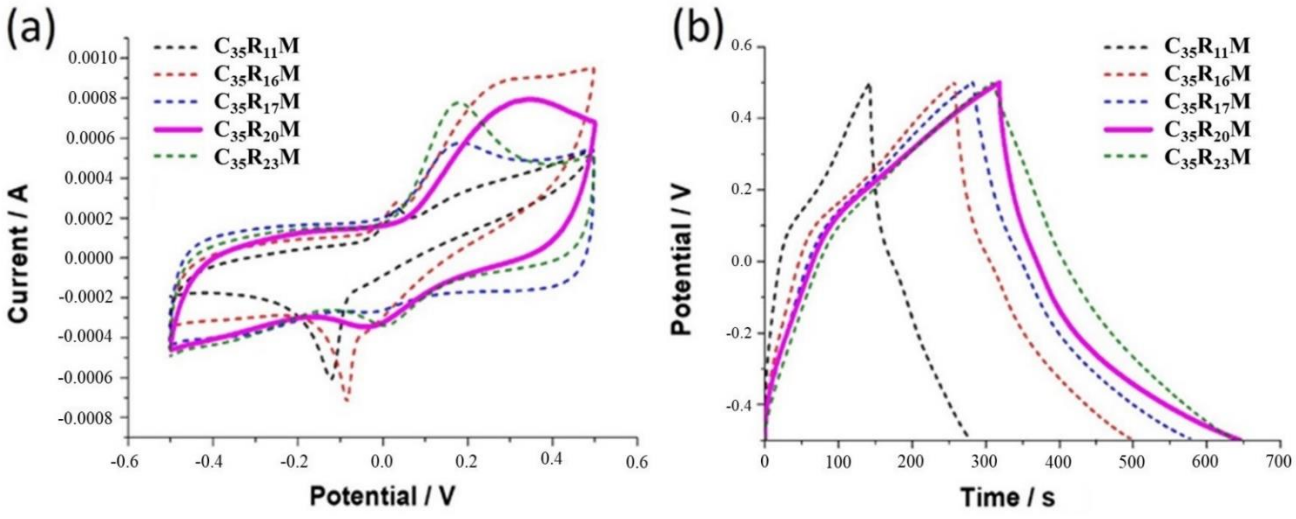

Figure 3. (**a**) CV curves of $C_{35}R_yM$ electrodes with various Ru contents, at a scan rate of 10 mV s^{-1}, and (**b**) GCD curves of $C_{35}R_yM$ electrodes with various Ru contents, at a current density of 1 A·g^{-1}.

It is evident in Figure 3a,b that the specific capacitance is increased with the Ru content in the nanocomposites. Better cycling performance is essential for the pseudo-capacitors to validate the mechanical stability of the electrode and active material degradability. As we can see from the CV curve, the $C_{35}R_{20}M$ with 20 wt% Ru displays a nearly rectangular cyclic voltammetry (CV) curve, with a maximum integrated area, indicating that the optimal Ru content delivers a high specific capacitance of 359.89 $F \cdot g^{-1}$. In addition, the GCD curves of the obtained samples in Figure 3b also support this fact, with a longer cycle time than the other samples. The calculated value of specific capacitance based on the obtained GCD curve is 326.92 $F \cdot g^{-1}$. It implies a much higher redox activity and capacity of the hybrid electrode. The appearance of maximum oxidation and minimum reduction peaks in Figure 3a confirms that the inclusion of metal oxides on the MWCNT surface play a vital role in improving the electrochemical performance.

The GCD curves in Figure 3b exhibit the asymmetric shape of charge and discharge half cycle, demonstrating a pseudocapacitive behavior, and it also confirms the presence of RuO_2 in the nanocomposite. In a three-electrode system, the specific capacitance of electrode materials can be calculated from the GCD plots according to Equation (2). The calculated specific capacitance values based on the CV curves and GCD curves of $C_{35}R_{20}M$ with 35% of Cu and various Ru content are respectively given in Table 1.

Table 1. The specific capacitances R_s and R_{ct} of the C_xR_yM electrodes evaluated by CV curves, GCD curves and Nyquist plots with various contents of Ru.

Specimen Designation	Ru Content (%) *	Specific Capacitance (F/g) by CV Curves	Specific Capacitance (F/g) by GCD Curves	R_s (Ω)	R_{ct} (Ω)
$C_{35}R_{11}M$	11	228.38	144.06	2.193	1502
$C_{35}R_{16}M$	16	257.67	259.44	2.747	59
$C_{35}R_{17}M$	17	272.15	295.23	2.442	4
$C_{35}R_{20}M$	20	359.89	326.92	2.271	5
$C_{35}R_{23}M$	23	300.98	323.82	2.261	1

*: the wt% were rounded to one digit.

The observed high specific capacitance of the $C_{35}R_{20}M$ nanocomposite could be attributed to the optimal dispersion of nano-sized RuO_2/CuO particles. The improved redox reactions occur at the surface of RuO_2 through a faradaic charge transfer between electrolyte and electrode, which enhances the specific capacitance of the nanocomposites. The presence of RuO_2 on the surface of MWCNTs modifies the structure and morphology of MWCNTs, which also allows improving the electrochemical reactions and improves the efficiency [33]. The tubular structure and the porous morphology of MWCNTs decrease the diffusion resistance and facilitate the transport and anchoring of NPs in the nanocomposites. The MWCNTs modified with RuO_2 at the surface inhibit fast electron-transfer kinetics and help the considerable change in their electrical conductivity.

It is also evident from the curves that the inclusion of RuO_2 could increase the conductivity of the sample at a certain level and thus increase the specific capacitance of this hybrid nanocomposite. Based on CV and GCD curves, it is clear that there is a higher load of RuO_2 because of the large number of particles that aggregate on the MWCNT surface, thus the conductivity is lowered and the function of MWCNT is also limited [34], which is unfavorable for better cycling performance. For Ru content of more than 20 wt%, RuO_2 NPs form an agglomerated structure and cover the surface of the MWCNTs, which can decrease the specific surface area and the specific capacitance. Moreover, the aggregation of RuO_2 NPs limits the utilization of the oxide particles and then leads to a significant reduction in its electrochemical performance [35]. The results suggest that a higher loading of Ru results in a low utilization of RuO_2 particles in the nanocomposite; however, the utilization is higher for a lower Ru content dispersed on the surface of the MWCNTs. The optimal loading of RuO_2 NPs on carbon materials causes a swift in the ion adsorption/desorption process and delivers high values of specific capacitance from the nanocomposite electrode.

The third set of experiments further approach the maximum capacitance by adjusting the Cu content based on 20% of Ru on MWCNT. Cyclic voltammetric and galvanostatic charge/discharge plots of the $Cu_xRu_{20}M$ electrodes with 20 wt% Ru and various Cu contents are illustrated in Figure 4a,b, respectively. For CV, the mass of active material used is 0.1 mg with an applied potential between −0.5 V to 0.5 V and the scan rate of 10 $mV{\cdot}s^{-1}$ and, for GCD, the applied charge/discharge current is 0.1 mA. Based on the curves in Figure 4a,b, the lowest Cu content (7%) in the nanocomposite has a wider rectangular CV curve and longer cycle times in the GCD curve than others, thus indicating that this sample has the highest specific capacitance. From Figure 4a,b and Table 2, we can observe that, by adding an optimal Cu content, the nanocomposite exhibits maximum specific capacitance of 363.88 $F{\cdot}g^{-1}$ and 461.59 $F{\cdot}g^{-1}$. This could be the reason for adding a small amount of CuO NPs into the nanocomposites, which generates an effective conductive network with MWCNTs. In addition to the RuO_2 particles, better interfacial attachments were observed between CNT and CuO NPs in the nanocomposite, caused by the strong interaction among nanotubes and CuO containing carboxyl groups and a few hydroxyl groups, respectively. The discharge curve in GCD for the $C_xR_{20}M$hybrid nanocomposite with 7% Cu content displayed a slow potential decay in Figure 4b. Table S4 compares the work conducted on copper oxides, ruthenium oxides and a carbon-based composite with our present work [19,36–40].

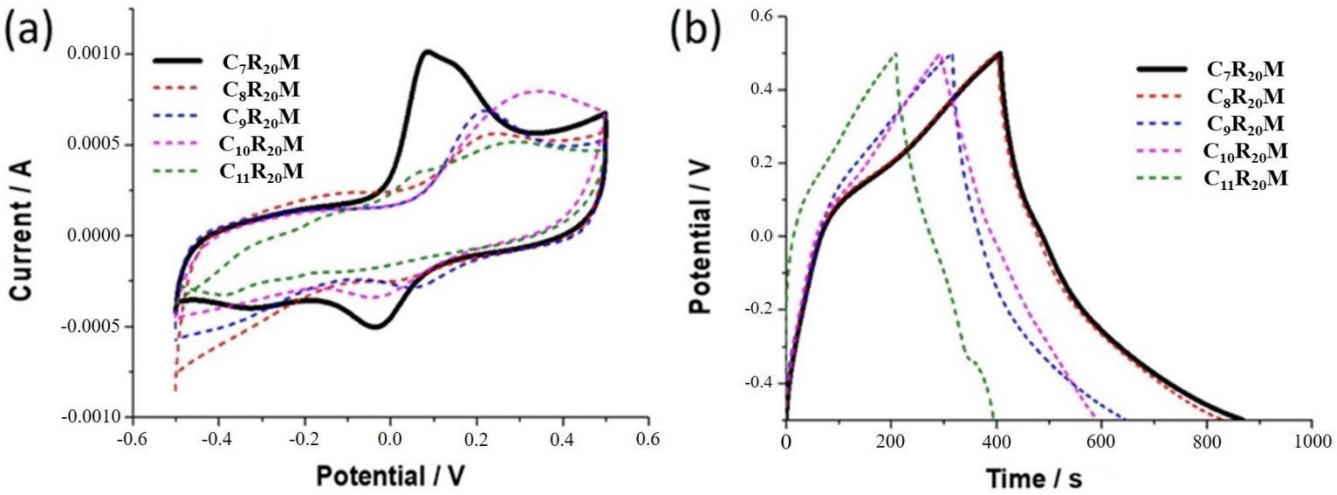

Figure 4. (**a**) CV curves of $C_xR_{20}M$electrodes with various Cu contents, at a scan rate of 10 $mV{\cdot}s^{-1}$, and (**b**) GCD curves of $C_xR_{20}M$ electrodes with various Cu contents, at a current density of 1 $A{\cdot}g^{-1}$.

Table 2. The specific capacitances R_s and R_{ct} of the $C_xR_{20}M$ electrodes evaluated by CV curves, GCD curves and Nyquist plots, with various contents of Cu.

Specimen Designation	Cu Content (%) *	Specific Capacitance (F/g) by CV Curves	Specific Capacitance (F/g) by GCD Curves	R_s (Ω)	R_{ct} (Ω)
$C_7R_{20}M$	7	363.88	461.59	2.259	2
$C_8R_{20}M$	8	343.70	437.15	2.426	3
$C_9R_{20}M$	9	323.90	326.92	2.291	9
$C_{10}R_{20}M$	10	301.91	305.63	2.260	251
$C_{11}R_{20}M$	11	212.94	210.65	2.095	583

*: the wt% were rounded to one digit.

The EIS technique was conducted to more precisely characterize the electrochemical behavior of C_xR_yM electrodes. From Figure 5a,b, it can be observed that all samples show a semicircle in the high-frequency region and a straight line in the low frequency region. A straight line found in the Nyquist plot for the $C_9R_{20}M$ nanocomposite electrodes indicates

that the MWCNTs still retain their electron-transfer capability after the surface modification by the CuO and RuO_2 NPs. The faradic charge-transfer resistances (R_{ct}) can be estimated from the diameter of the semicircle in the high-frequency region [41] and are listed in Table 2. It can be observed that $C_xR_{20}M$ possesses a moderate R_{ct} value than those with other Ru values, indicating an enhanced electron transport efficiency. In Table 2, it can be seen that $C_xR_{20}M$ with 7% of Cu content possesses a moderate R_{ct} value than those with other Cu values, indicating an enhanced electron transport efficiency.

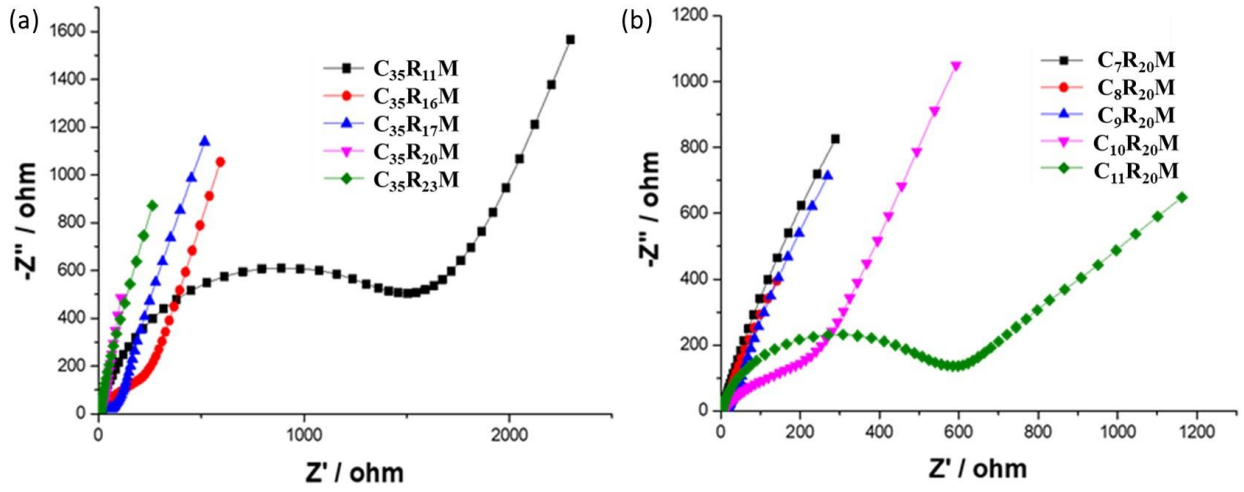

Figure 5. Nyquist plot of the (**a**) $C_{35}R_yM$ and (**b**) $C_xR_{20}M$ electrodes with various contents of Ru and Cu, respectively ((**a**) Ru and (**b**) Cu).

In addition to the high specific capacitance, the $C_7R_{20}M$ electrodes also established outstanding high-power density and high-energy density performance, as shown in the Ragone plot in Figure 6. The electrochemical test results for the as-prepared CuO/RuO_2/MWCNT nanocomposite nanostructures with a controlled level of CuO/RuO_2 NPs on the surfaces of the MWCNTs show that the ternary nanocomposite can be used as superior electrode materials for electrochemical (hybrid) capacitors with a high specific capacitance and significant high-power and high-energy capabilities.

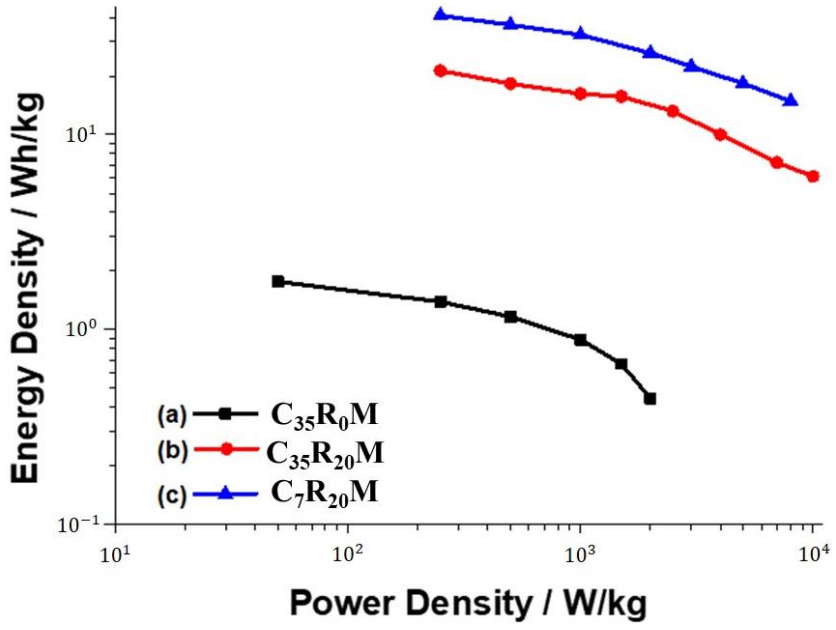

Figure 6. Ragone plot of (a) $C_{35}R_0M$ (b) $C_{35}R_{20}M$ and (c) $C_7R_{20}M$ electrodes.

4. Conclusions

The hydrothermal method is a simple and efficient in situ synthesis technique that was utilized to decorate binary metal oxides NPs, namely RuO_2 and CuO, on MWCNTs for investigation as an electrode material in a supercapacitor. This method offers several significant advantages: low cost, high crystallinity, narrow particle size distribution and varying in morphology by the adjustment of precursor metal basis concentration. The structural, morphological and compositional analyses using FE-SEM, TGA and EDX-mapping have confirmed the successful synthesis of the proposed CuO/RuO_2/MWCNT electrodes. The highest value of specific capacitance was observed for the CuO/RuO_2/MWCNT nanocomposite with the percentage of 7%, 20% and 60% respectively, for Cu, Ru and CNT (461.59 F/g at 10 $mV \cdot s^{-1}$ scan rate) compared to all other electrodes prepared in this study. The synergic interaction of each element in this CuO/RuO_2/MWCNT ternary nanocomposite of CuO/RuO_2/MWCNTs is ascribed to the efficient electrochemical characteristics observed in this study.

Supplementary Materials: The following supporting information can be downloaded at: https://www.mdpi.com/article/10.3390/catal12010023/s1. Figure S1: EDS Mapping images of $C_{35}R_yM$ electrodes with (a) 11, (b) 16, (c) 17, (d) 20, and (e) 23 wt% Ru; Figure S2: EDS mapping of $C_xR_{20}M$ electrodes with (a) 7, (b) 8, (c) 9, (d) 10, and (e) 11 wt% Cu; Figure S3: The TGA curves of (a) the $C_{35}R_yM$ nanocomposites with various content of Ru and (b) the $C_xR_{20}M$ nanocomposites with various content of Cu; Table S1: The residual weight percentage and thermal stability of the $C_{35}R_yM$ nanocomposites with various content of Ru; Table S2: The residual weight percentage and thermal stability of the $C_xR_{20}M$ nanocomposites with various content of Cu; Figure S4: (a) CV curves of C_xR_0M electrodes with various Ru content, at a scan rate of 10 $mV \cdot s^{-1}$, (b) GCD curves of C_xR_0M electrodes with various Ru content, at a current density of 1 $A \cdot g^{-1}$; Table S3: The specific capacitance of the C_xR_0M electrodes valuated by CV curves and GCD curves, with various content of Cu; Table S4: Comparison of electrochemical properties of CuO/RuO_2/MWCNT with samples reported in literature; Figure S5: Cyclic stability test of $C_7R_{20}M$ electrode.

Author Contributions: Review and editing, investigation, Y.-C.C.; conceptualization, methodology, formal analysis, A.J.; supervision, writing—original draft preparation, L.S.; data curation, formal analysis, P.-R.C., B.-C.X. and P.-J.X.; project administration, funding acquisition, resources, A.-Y.L. All authors have read and agreed to the published version of the manuscript.

Funding: This research was funded by the Ministry of Science and Technology (MOST 108-2221-E-167-009-MY3; Taiwan).

Acknowledgments: The authors thank the BET, XRD, and SEM/EDS measurement services provided by the Green Energy and Engineering Materials Research Center of National Chin-Yi University of Technology (NCUT), Taiwan.

Conflicts of Interest: The authors declare no conflict of interest.

References

1. Saravanan, L.; Tseng, C.-M.; Chia-Chia, C.; Chung, Y.-C.; Chung, Y.-C.; Lin, C.-Y.; Lo, A.-Y. Pt–RuO–SnO/CMK-3 composite electrocatalysts for the methanol oxidation reaction. *C. R. Chim.* **2020**, *23*, 343–356. [CrossRef]
2. Lo, A.-Y.; Taghipour, F. Review and prospects of microporous zeolite catalysts for CO_2 photoreduction. *Appl. Mater. Today* **2021**, *23*, 101042. [CrossRef]
3. Lo, A.-Y.; Chang, C.-C.; Lai, Y.-W.; Chen, P.-R.; Xu, B.-C. Improving the supercapacitor performance by dispersing SiO_2 microspheres in electrodes. *ACS Omega* **2020**, *5*, 11522–11528. [CrossRef] [PubMed]
4. Lo, A.-Y.; Saravanan, L.; Tseng, C.-M.; Wang, F.-K.; Huang, J.-T. Effect of composition ratios on the performance of Graphene/Carbon nanotube/Manganese oxide composites toward supercapacitor applications. *ACS Omega* **2020**, *5*, 578–587. [CrossRef]
5. Wang, G.; Zhang, L.; Zhang, J. A review of electrode materials for electrochemical supercapacitors. *Chem. Soc. Rev.* **2012**, *41*, 797–828. [CrossRef] [PubMed]
6. Sevilla, M.; Mokaya, R. Energy storage applications of activated carbons: Supercapacitors and hydrogen storage. *Energy Environ. Sci.* **2014**, *7*, 1250–1280. [CrossRef]
7. Liu, Z.; Yuan, X.; Zhang, S.; Wang, J.; Huang, Q.; Yu, N.; Zhu, Y.; Fu, L.; Wang, F.; Chen, Y.; et al. Three-dimensional ordered porous electrode materials for electrochemical energy storage. *NPG Asia Mater.* **2019**, *11*, 12. [CrossRef]

8. Ricketts, B.W.; Ton-That, C. Self-discharge of carbon-based supercapacitors with organic electrolytes. *J. Power Sour.* **2000**, *89*, 64–69. [CrossRef]
9. Burke, A. Ultracapacitor technologies and application in hybrid and electric vehicles. *Int. J. Energy Res.* **2010**, *34*, 133–151. [CrossRef]
10. Yu, G.; Xie, X.; Pan, L.; Bao, Z.; Cui, Y. Hybrid nanostructured materials for high-performance electrochemical capacitors. *Nano Energy* **2013**, *2*, 213–234. [CrossRef]
11. Li, X.; Wei, B. Supercapacitors based on nanostructured carbon. *Nano Energy* **2013**, *2*, 159–173. [CrossRef]
12. Dubal, D.P.; Kim, J.G.; Kim, Y.; Holze, R.; Lokhande, C.D.; Kim, W.B. Supercapacitors based on flexible substrates: An Overview. *Energy Technol.* **2014**, *2*, 325–341. [CrossRef]
13. An, G.H. Metal ion capacitor composed of the thin-walled surfaces enabling high-rate performance and long cycling stability. *Curr. Appl. Phys.* **2020**, *20*, 605–610. [CrossRef]
14. Lang, X.; Hirata, A.; Fujita, T.; Chen, M. Nanoporous metal/oxide hybrid electrodes for electrochemical supercapacitors. *Nat. Nanotechnol.* **2011**, *6*, 232–236. [CrossRef] [PubMed]
15. Li, X.; He, H. Hydrous RuO_2 nanoparticles coated on $Co(OH)_2$ nanoflakes as advanced electrode material of supercapacitors. *Appl. Surf. Sci.* **2019**, *470*, 306–317. [CrossRef]
16. Dinh, T.M.; Achour, A.; Vizireanu, S.; Dinescu, G.; Nistor, L.; Armstrong, K.; Guay, D.; Pech, D. Hydrous RuO_2/carbon nanowalls hierarchical structures for all-solid-state ultrahigh-energy-density micro-supercapacitors. *Nano Energy* **2014**, *10*, 288–294. [CrossRef]
17. Bi, R.-R.; Wu, X.-L.; Cao, F.-F.; Jiang, L.-Y.; Guo, Y.-G.; Wan, L.-J. Highly dispersed RuO_2 nanoparticles on carbon nanotubes: Facile synthesis and enhanced supercapacitance performance. *J. Phys. Chem. C* **2010**, *114*, 2448–2451. [CrossRef]
18. Zhang, Y.; Park, S.-J. Incorporation of RuO_2 into charcoal-derived carbon with controllable microporosity by CO_2 activation for high-performance supercapacitor. *Carbon* **2017**, *122*, 287–297. [CrossRef]
19. Ye, J.-S.; Cui, H.F.; Liu, X.; Lim, T.M.; Zhang, W.-D.; Sheu, F.-S. Preparation and characterization of aligned carbon nanotube–ruthenium oxide nanocomposites for supercapacitors. *Small* **2005**, *1*, 560–565. [CrossRef]
20. Chuang, C.-M.; Huang, C.-W.; Teng, H.; Ting, J.-M. Hydrothermally synthesized RuO_2/Carbon nanofibers composites for use in high-rate supercapacitor electrodes. *Compos. Sci. Technol.* **2012**, *72*, 1524–1529. [CrossRef]
21. Jiang, H.; Ma, J.; Li, C. Mesoporous carbon incorporated metal oxide nanomaterials as supercapacitor electrodes. *Adv. Mater.* **2012**, *24*, 4197–4202. [CrossRef]
22. Anandan, S.; Yang, S. Emergent methods to synthesize and characterize semiconductor CuO nanoparticles with various morphologies—An overview. *J. Exp. Nanosci.* **2007**, *2*, 23–56. [CrossRef]
23. Zhang, R.; Liu, J.; Guo, H.; Tong, X. Synthesis of CuO nanowire arrays as high-performance electrode for lithium ion batteries. *Mater. Lett.* **2015**, *139*, 55–58. [CrossRef]
24. Ruan, J.-j.; Huo, Y.-q.; Hu, B. Three-dimensional $Ni(OH)_2/Cu_2O/CuO$ porous cluster grown on nickel foam for high performance supercapacitor. *Electrochim. Acta* **2016**, *215*, 108–113. [CrossRef]
25. Wang, Q.; Zhang, Y.; Xiao, J.; Jiang, H.; Hu, T.; Meng, C. Copper oxide/cuprous oxide/hierarchical porous biomass-derived carbon hybrid composites for high-performance supercapacitor electrode. *J. Alloys Compd.* **2019**, *782*, 1103–1113. [CrossRef]
26. Fisher, R.A.; Watt, M.R.; Jud Ready, W. Functionalized Carbon Nanotube Supercapacitor Electrodes: A Review on Pseudocapacitive Materials. *ECS J. Solid State Sci. Technol.* **2013**, *2*, M3170–M3177. [CrossRef]
27. Cui, X.; Zhou, J.; Ye, Z.; Chen, H.; Li, L.; Ruan, M.; Shi, J. Selective catalytic oxidation of ammonia to nitrogen over mesoporous CuO/RuO_2 synthesized by co-nanocasting-replication method. *J. Catal.* **2010**, *270*, 310–317. [CrossRef]
28. Hosseini, M.G.; Shahryari, E. Synthesis, characterization and electrochemical study of graphene oxide-multi walled carbon nanotube-manganese oxide-polyaniline electrode as supercapacitor. *J. Mater. Sci. Technol.* **2016**, *32*, 763–773. [CrossRef]
29. Manasrah, A.D.; Al-Mubaiyedh, U.A.; Laui, T.; Ben-Mansour, R.; Al-Marri, M.J.; Almanassra, I.W.; Abdala, A.; Atieh, M.A. Heat transfer enhancement of nanofluids using iron nanoparticles decorated carbon nanotubes. *Appl. Therm. Eng.* **2016**, *107*, 1008–1018. [CrossRef]
30. Li, H.B.; Yu, M.H.; Wang, F.X.; Liu, P.; Liang, Y.; Xiao, J.; Wang, C.X.; Tong, Y.X.; Yang, G.W. Amorphous nickel hydroxide nanospheres with ultrahigh capacitance and energy density as electrochemical pseudocapacitor materials. *Nat. Commun.* **2013**, *4*, 1894. [CrossRef]
31. Han, Z.J.; Pineda, S.; Murdock, A.T.; Seo, D.H.; Ostrikov, K.; Bendavid, A. RuO_2-coated vertical graphene hybrid electrodes for high-performance solid-state supercapacitors. *J. Mater. Chem. A* **2017**, *5*, 17293–17301. [CrossRef]
32. Mohan, R.; Paulose, R. Influence of ferrites nanoparticles anchored on CNT hybrid nanocomposites for high-performance energy storage applications. *J. Electron. Mater.* **2018**, *47*, 6878–6885. [CrossRef]
33. Su, Y.C.; Chen, C.A.; Chen, Y.M.; Huang, Y.S.; Lee, K.Y.; Tiong, K.K. Characterization of RuO_2 nanocrystals deposited on carbon nanotubes by reactive sputtering. *J. Alloys Compd.* **2011**, *509*, 2011–2015. [CrossRef]
34. Yang, L.; Zhang, J.; Zhang, Y.; Zhao, Y.; Yin, H.; Hua, Q.; Yuan, J.; Tang, J. A ternary composite RuO_2@SWCNT/graphene for high performance electrochemical capacitors. *Mater. Lett.* **2020**, *259*, 126860. [CrossRef]
35. Kong, S.; Cheng, K.; Ouyang, T.; Gao, Y.; Ye, K.; Wang, G.; Cao, D. Facile electrodepositing processed of RuO_2-graphene nanosheets-CNT composites as a binder-free electrode for electrochemical supercapacitors. *Electrochim. Acta* **2017**, *246*, 433–442. [CrossRef]

36. Zhang, X.; Shi, W.; Zhu, J.; Kharistal, D.J.; Zhao, W.; Lalia, B.S.; Hng, H.H.; Yan, Q. High-Power and High-Energy-Density Flexible Pseudocapacitor Electrodes Made from Porous CuO Nanobelts and Single-Walled Carbon Nanotubes. *ACS Nano* **2011**, *5*, 2013–2019. [CrossRef]
37. Kavil, J.; Anjana, P.M.; Joshy, D.; Babu, A.; Raj, G.; Periyat, P.; Rakhi, R.B. g-C_3N_4/CuO and g-C_3N_4/Co_3O_4 nanohybrid structures as efficient electrode materials in symmetric supercapacitors. *RSC Adv.* **2019**, *9*, 38430–38437. [CrossRef]
38. Paulose, R.; Raja, M. CuO nanoparticles/multi-walled carbon nanotubes (MWCNTs) nanocomposites for flexible supercapacitors. *J. Nanosci. Nanotechnol.* **2019**, *19*, 8151–8156. [CrossRef]
39. Asim, S.; Javed, M.S.; Hussain, S.; Rana, M.; Iram, F.; Lv, D.; Hashim, M.; Saleem, M.; Khalid, M.; Jawaria, R.; et al. RuO_2 nanorods decorated CNTs grown carbon cloth as a free standing electrode for supercapacitor and lithium ion batteries. *Electrochim. Acta* **2019**, *326*, 135009. [CrossRef]
40. Zhang, P.; Liu, X.; He, H.; Peng, Y.; Wu, Y. Engineering RuO_2 on $CuCo_2O_4$/CuO nanoneedles as multifunctional electrodes for the hybrid supercapacitors and water oxidation catalysis. *J. Alloys Compd.* **2020**, *832*, 154962. [CrossRef]
41. Zhao, J.; Li, Z.; Yuan, X.; Shen, T.; Lin, L.; Zhang, M.; Meng, A.; Li, Q. Novel core-shell multi-dimensional hybrid nanoarchitectures consisting of $Co(OH)_2$ nanoparticles/Ni_3S_2 nanosheets grown on SiC nanowire networks for high-performance asymmetric supercapacitors. *Chem. Eng. Sci.* **2019**, *357*, 21–32. [CrossRef]